Physics Letters A 526 (2024) 129963

Contents lists available at ScienceDirect

Physics Letters A

journal homepage: www.elsevier.com/locate/pla

Letter

Disordered Heisenberg XYZ magnetic chains with exponential correlations: Localization and quantum state transfer

D.B. Fonseca [a], A.L.R. Barbosa [a], F. Moraes [a], G.M.A. Almeida [b], F.A.B.F. de Moura [b,*]

[a] Departamento de Física, Universidade Federal Rural de Pernambuco, 52171-900, Recife, PE, Brazil
[b] Instituto de Física, Universidade Federal de Alagoas, Maceió AL 57072-970, Brazil

ARTICLE INFO

Communicated by M.G.A. Paris

Keywords:
Spin chain
Correlated disorder
Quantum-state transfer

ABSTRACT

Our study investigates the Quantum State Transfer Protocol within a one-dimensional quantum Heisenberg spin chain model that features exponentially correlated disorder in the spin coupling distribution. We conducted extensive numerical simulations to explore how varying degrees of correlation impact the transfer of quantum states through this model of a quantum channel. Our results demonstrate that the extent of correlation significantly influences quantum communication along the channel. Specifically, we observed that in the strongly correlated regime, quantum communication remains largely unaffected even in large systems. These findings are interpreted in the context of the localization properties inherent to the disordered channel.

1. Introduction

Among the many challenges in the field of quantum information processing [1–8], developing robust quantum state transfer protocols (QSTP) between processing units is of paramount importance. The central goal is to prepare an arbitrary quantum state at one location and determine if the system's natural temporal evolution can reliably transfer it to another site with high fidelity. Since S. Bose's proposal of using spin-1/2 chains as channels for short-distance communication, numerous QSTP schemes have been introduced.

One promising strategy involves engineering the couplings within the spin chain such that quantum state transfer and entanglement generation become independent of system size [9,10]. This approach typically requires the inclusion of long-range interactions and an optimization scheme to approximate the ideal behavior while maintaining strong interaction strengths. An essential aspect of this process is isolating the sender and receiver from the remainder of the chain. Research by Gualdi and Lorenzo [11,12] demonstrates that this method scales effectively to larger systems, with the fidelity of QSTP remaining constant over time and approaching optimal values. Their findings suggest that the QSTP fidelity remains invariant as the system size increases, making this approach highly scalable.

Reference [13] described an XY model with long-range interactions within the framework of ion traps. The authors demonstrated that such a system provides a quantum state transfer protocol with qubit encoding that maintains high fidelity. Additionally, Reference [14] demonstrated a quantum matter link that transfers ion qubits between adjacent quantum computer modules. Ion transport between these modules is achieved at a rate of 2424 s^{-1}, with minimal infidelity related to ion loss. Furthermore, the authors showed that the link does not measurably impact the phase coherence of the qubit. This quantum matter link represents a practical mechanism for connecting quantum charge-coupled devices.

In the context of quantum state transfer in low-dimensional systems, a critical factor to consider is the effect of disorder. The authors of Ref. [15] investigated the impact of static imperfections introduced during the sample manufacturing process under the quantum state transfer protocol. They demonstrated that performance can be improved by judiciously selecting the Hamiltonian and implementing encoding and decoding procedures in small regions at either end of the chain. Their findings also indicate that encoding solely within the single-excitation subspace is optimal and significantly enhances the system's operational regime. Additionally, Ref. [16] explored the feasibility of quantum state transfer in a one-dimensional random lattice with varying levels of control resources. It was shown that with appropriate signals applied to the two ends of the lattice, perfect state transfer can be achieved up to a certain level of disorder strength. Beyond this threshold, disorder would typically prevent the propagation of a generic quantum state through the lattice.

In this context, our research investigates the quantum state transfer protocol (QSTP) in a one-dimensional spin chain characterized by a spin coupling distribution with exponentially correlated disorder.

* Corresponding author.
E-mail address: fidelis@fis.ufal.br (F.A.B.F. de Moura).

https://doi.org/10.1016/j.physleta.2024.129963
Received 30 July 2024; Received in revised form 30 September 2024; Accepted 3 October 2024

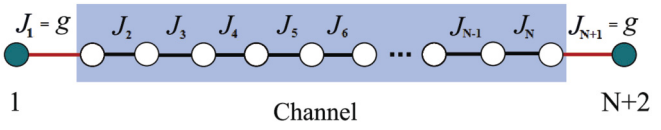

Fig. 1. The system consists of two spins (green), labeled sites 1 and $N+2$, which are coupled to the channel by a g exchange interaction. The channel is represented by a N spins (white) series connected by a correlated exchange interaction J_i.

Ref. [17] reveals that a distinctive multifractal regime emerges in a one-dimensional electronic chain when the disorder strength surpasses a certain threshold, specifically under exponentially correlated disorder. This phenomenon is anticipated to impact the QSTP in a one-dimensional spin chain. Our findings show that the degree of correlation significantly influences the transmission of quantum states through this model. Our numerical results indicate that quantum communication along the channel remains relatively stable in the presence of strong correlations, even for large systems.

2. Model

We consider a quantum Heisenberg model with $N+2$ spins–1/2 in a 1D channel with a correlated disorder in exchange energies, as illustrated in Fig. 1. The Hamiltonian of spin waves is given by

$$H_S = -J_1\vec{S}_1\cdot\vec{S}_2 - \sum_{\langle i=2,\ldots,N+1\rangle} J_i\vec{S}_i\cdot\vec{S}_{i+1} - J_{N+1}\vec{S}_{N+1}\cdot\vec{S}_{N+2}, \tag{1}$$

where we consider $\hbar = 1$. We can write this Hamiltonian in a subspace spanned by $|i\rangle \equiv \left|\downarrow_1,\downarrow_2,\ldots,\downarrow_{i-1},\uparrow_i,\downarrow_{i+1},\ldots,\downarrow_{N+2}\right\rangle$ [18–20], where $|i\rangle$ denotes a single spin flipped at the ith spin. The spins 1 and $N+2$ are denoting the source $\boldsymbol{S}$ and receiver $\boldsymbol{R}$. The hopping J_i denotes the exchange energy between spins i and $i+1$. We consider the hopping $J_1 = J_{N+1} = g$ while the remaining hopping J_i with $i = 2,\ldots,N+1$ assume correlated random values given by

$$J_i = 0.5\tanh\left(\sum_m Z_m \times \exp\left[\frac{-d_{i,m}}{\lambda N}\right]\right) + 1. \tag{2}$$

The parameter Z_m is a random number uniformly distributed between -0.5 and 0.5, $d_{i,m}$ is the Euclidean distance from i index to m index, and λ controls the correlation length (λN). Thus, J_i is a correlated random number range in the interval $[0.5, 1.5]$. Fig. 2 shows the behavior of hopping J_i as a function of index i for different $N\lambda$ values. For $N\lambda \approx 1$, the J_i behaves as an uncorrelated sequence of numbers. On the other hand, when $N\lambda$ has increased, the one behaves as a correlated sequence of numbers saturated for larger $N\lambda$.

Following Ref. [17], we assume correlations in the hopping that decay with the distance as

$$\rho(r = |i-j|) = \frac{\langle J_iJ_j\rangle - \langle J_i\rangle\langle J_j\rangle}{\langle J_i^2\rangle - \langle J_i\rangle^2}. \tag{3}$$

The behavior of $\rho(r)$ as a function of r can be observed in Fig. 3. For $N\lambda = 1$, we note that $\rho(r)$ goes to zero when $r > 1$. As the correlated parameter $N\lambda$ increases, we observed that $\rho(r)$ remains larger than zero in the distance $r < r_0$; we also observed that r_0 increases as $N\lambda$ is increased. Therefore, as we can see in the mathematical definition of the sequence J_i and the $\rho(r)$ results, the quantity $N\lambda$ controls the degree of correlations within the channel's disorder distribution.

The channel's disorder distribution deserves still another investigation related to its local disorder. The local disorder Δ_{n_0} can be computed as follows: i) First, we divide the disorder distribution within the channel into segments of size n_0; for each segment, we calculate the deviation of J_i as $\delta_k = \sqrt{\langle J_i^2\rangle_k - \langle J_i\rangle_k^2}$ where k run over all segments (i.e. $k = 1,2,3,\ldots,N/n_0$). The local disorder is defined as $\Delta_{n_0} = \sum_k \delta_k/(N/n_0)$.

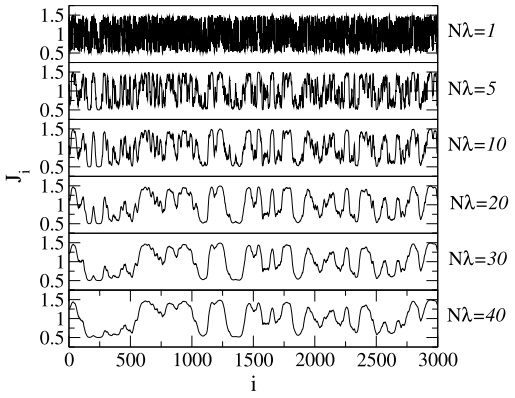

Fig. 2. The hopping J_i, Eq. (2), as a function of index i for different value of $N\lambda$.

In our calculations, we will use $N/n_0 = 10$. The results considering $N = 2000$, 4000 and $N\lambda = 1$ up to 2000 are showed in Fig. 4. For $N\lambda \approx 1$, the local disorder becomes roughly as the same order as an uncorrelated disordered sequence of numbers within the interval $[0.5, 1.5]$. However, as the correlated parameter increases (i.e., $N\lambda \gg 1$), the local disorder decreases considerably and roughly saturates for larger $N\lambda$. Therefore, the presence of correlations within the disorder distribution within the channel decreases the intensity of disorder locally; however, for finite N/λ, the system still contains disorder (even if it is a very weak disorder). We emphasize that the results of Δ_{n_0} are qualitatively independent of the value of N/n_0 we choose.

We are interested in the efficiency of QSTP from the site 1 to site $N+2$ for spin chains with correlated hopping Hamiltonians; see Fig. 1. We discuss next several observables that characterize the performance of QSTP. Therefore, we use the temporal evolution operator $\Theta(t) = e^{-i\mathcal{H}t}$ [21,22] in the prepared state $|\Psi(0)\rangle = |\boldsymbol{S}\rangle$. To obtain the temporal evolution of the prepared state, we apply the operator to $|\Psi(0)\rangle$ as follows $|\Psi(t)\rangle = \Theta(t)\,|\Psi(0)\rangle = \sum_{i=1}^{N+2} f_i(t)\,|i\rangle$, which return the state $|\Psi(t)\rangle$ at any time t. The amplitude of transition of excitation from site $\boldsymbol{S}$ to site $\boldsymbol{R}$, $f_{N+2}(t) = \langle \boldsymbol{R}|\, e^{-i\mathcal{H}\frac{t}{\hbar}}\,|\boldsymbol{S}\rangle$, is used to quantify the performance of QSTP. We emphasize that this type of calculation needs to be performed for long times, the relevant timescale of the transfer in weak-coupling models ($g \ll 1$) typically scales as $\sim g^{-2}$ [18,20,23]. This computational procedure using the time evolution operator is formally exact, depending only on the diagonalization of the Hamiltonian. Therefore, this procedure used here, due to its analytical nature, ensures the temporal evolution of the wave packet for long times without degradation of the wave function's norm. The time scale is divided into time steps Δt, meaning that given the initial state, we calculate the state of the system at times $t = \Delta t, 2\Delta t, 3\Delta t$, and so on. In our studies, we considered various values for the time step Δt (ranging from reasonably small values such as $\Delta t < 1$ to larger values around $\Delta t \approx 100$ or greater). The results for the average physical quantities were qualitatively and quantitatively similar. As a result, most of our studies were conducted with $\Delta t \approx 100$.

3. Results and discussion

Before we show our analysis of the transference of quantum states within our model, we will analyze the localization properties of the channel (i.e., the inner sites between the interval $2 \le i \le N+1$). We diagonalize the Hamiltonian of the track for systems with size $N = 1000$ up to $N = 16000$ sites. We calculate the participation number defined as $P_{E_i} = \left(\sum_n |f_n^{E_i}|^4\right)^{-1}$ where $f_n^{E_i}$ is the wave-function component associated with the eigenvalue $|E_i\rangle = \sum_n f_n^{E_i}|n\rangle$. We emphasize that participation measures the size of the eigenvectors; for localized states, we have P_{E_i} equal to a few sites (and this number is generally independent of N).

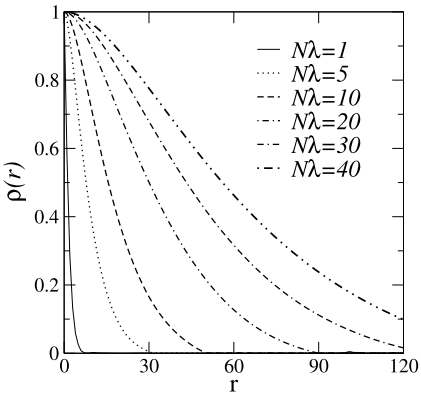

Fig. 3. Correlation $\rho(r)$ of Hopping J_i, Eq. (3), as a function of distance r for several values of $N\lambda$.

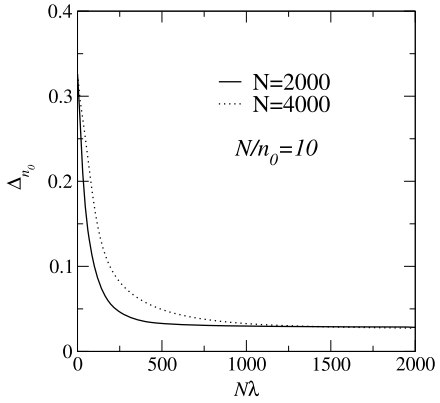

Fig. 4. The local disorder Δ_{n_0} versus $N\lambda$ for $N = 2000$ and 4000. The parameter N/n_0 was considered equal to 10 and $N\lambda = 1$ up to 2000.

However, the participation number is proportional to the system size for extended states. In our work, we focus the analysis on the mean participation number $P(E)$ defined as $P(E) = \sum_{|E_i - E| < \Delta E} P_E / N_E$ where N_E is the number of eigenfunction between the interval $[E - \Delta E, E + \Delta E]$.

In Fig. 5 we plot $P(E)$ as a function of E for $N = 1000$ up to 16000 for $N\lambda = 0.5$, 4, and 8. When $N\lambda = 0.5$, we are working with a weakly disorder distribution correlated. In this scenario, as N increases for $E > 0$, the scaled participation number P/N decreases. However, when $E = 0$, the scaled participation number remains mostly constant, which is consistent with prior research on the propagation magnon state at the band's bottom. For $N\lambda = 4$ and 8, our findings suggest that the participation number at the low-energy region is roughly proportional to N.

In Fig. 6, we analyze the finite size scaling of P as a function of N for several values of $N\lambda$ and N. We calculate the participation number for two energies, $E = 0.25$ and $E = 0.5$. Thus, we diagonalize the Hamiltonian around the energies (considering a small window of size 0.1) for systems up to $N = 76000$ sites to improve the finite size scaling. The finite size scaling was obtained to calculate $P \times N$ for several values of correlation degree ($N\lambda = 1, 2, 4, 8, 16, 32$) and obtain the typical localization length L_0 for each value of $N\lambda$. Therefore, we plotted the scaled variables P/L_0 versus N/L_0 and got a fine data-collapse of all dates, as shown in Fig. 6(a,b). We emphasize that L_0 was obtained as a value about the maximum participation number for each $N\lambda$. The explanation of this collapse is the single parameter scaling hypothesis that the possibility to write the participation number as $\langle P \rangle(N, \lambda) = L_0(N, \lambda) f[N/L_0]$. For $N > L_0$ the scaling function converges to a constant. For $N < L_0$ the scaling function becomes proportional to N/L_0 and, therefore, the participation is roughly proportional to N. Our calculations suggest that $L_0 \propto (N\lambda)^2$, as shown in Fig. 6(c).

We begin our analysis of quantum state transfer within our model. To follow Bose's protocol, it is essential that the diagonal terms for both the source S and the receiver R are identical to maintain the resonance proposed in Bose's protocol. In the context of our model, the diagonal terms for the source S and the receiver R (i.e., $H_{1,1}$ and $H_{N+2,N+2}$) are $(g + J_2)/2$ and $(g + J_N)/2$, respectively, and these values are clearly unequal. Therefore, to maintain resonance and adhere to Bose's protocol, we introduce a local magnetic field term, ensuring that the diagonal energies for the source and receiver are given by $\epsilon = H_{1,1} + h_1 = H_{N+2,N+2} + h_{N+2}$. By applying this local field to spins S and R, we can fix the diagonal terms at both S and R to a constant value ϵ. Notably, in our studies, ϵ is considered close to zero, as this energy region intensifies the effects of exponential correlations on the localization properties of the channel. Our initial analysis focuses on the role of the coupling g between the source and the receiver with the channel. In this numerical calculation, we consider spin chains with $N = 100$ spins in the channel and observe the time evolution of an initial state localized at site $\boldsymbol{S}$ (the first site of our model, also referred to as the "source," as illustrated in Fig. 1). The time evolution is calculated for up to 10^6 time units. To evaluate the potential for quantum transfer to the last site $\boldsymbol{R}$ (site $N + 2$, also called the "receiver"), we use Fidelity as a tool to quantify the success of state transfer [24].

$$F(t) = \frac{1}{2} + \frac{|f_{N+2}(t)|}{3} + \frac{|f_{N+2}(t)|^2}{6}. \tag{4}$$

We calculate the maximum Fidelity value $F_{max} = \langle max\{F(t)\} \rangle$ in the range of time within $[2 \times 10^5, 10^6]$. We stress that when a perfect state transfer occurs, we found $F = 1$; however, in the absence of quantum state transference, the Fidelity reaches the value $1/2$. In Fig. 7.(a), we plotted F_{max} versus g for several values of $N\lambda$. Our calculations suggest that to occur state transfer, the coupling g needs to be weak ($g \approx 0.01$), and the Fidelity can be close to 1 for strong correlate $N\lambda \geq 5$; otherwise, the state transfer will not take place (even for strongly correlated cases $N\lambda \gg 1$).

We also used the concurrence $C(t) = 2|f_1(t)||f_{N+2}(t)|$ [25] to analysis the existence of quantum-state transfer. This quantity measures the entanglement between the source and the receiver; $C(t) = 1$ means entangled states, and $C(t) = 0$ indicates the absence of entangled states. The maximum concurrence C_{max} is calculated in the same way as F_{max}. Fig. 7.(b) shows the concurrence as a function of g, which has a similar behavior of F. The concurrence presents entanglement at lower values of g and losing entanglement at higher values of g. Furthermore, the correlation increases the concurrence close to 1 for lower values of g.

To complement the analysis of the role played by the value of the coupling g, we observe the contributions of sites for the wave function and where the wave function is located; our main focus is observed whenever the wave function remains trapped in the $\boldsymbol{S}$ and $\boldsymbol{R}$ sites or on the channel. To do so, we use three quantities: i) time-dependent participation number $\xi(t) = \left(\sum_{i=1}^{N+2} |f_i(t)|^4\right)^{-1}$, where the function $\xi(t)$ has the same properties that were described to function $P(E_i)$ however, $\xi(t)$ is obtained using the time-dependent wave-packet; ii) the function $f_{SR} = |f_1(t)|^2 + |f_{N+2}(t)|^2$ that measures the fraction of amplitude of wave function is at the source and the receiver; iii) function $f_C = \sum_{i=2}^{N+1} |f_i(t)|^2$ that measures the fraction of amplitude of the wave function is in the channel. We emphasize that we analyzed these three quantities following the same procedure we have employed to compute F_{max} and C_{max} (i.e., we found the mean maximum value within the time interval $[2 \times 10^5, 10^6]$). In this complementary analysis, as depicted in Fig. 8.(a), we found the ξ_{max} value increases with increasing g. This suggests that as the coupling g increases, the initially localized state spreads along the channel. The delocalization hinders QST within the system, leading to a decrease in QST efficiency. It is unclear which specific sites contribute significantly to the wave function for weak coupling, but fortunately, functions f_{SR} and f_C can help identify them. As depicted in Fig. 8.(b), $\boldsymbol{S}$ and $\boldsymbol{R}$ sites are where the wave function is predominantly

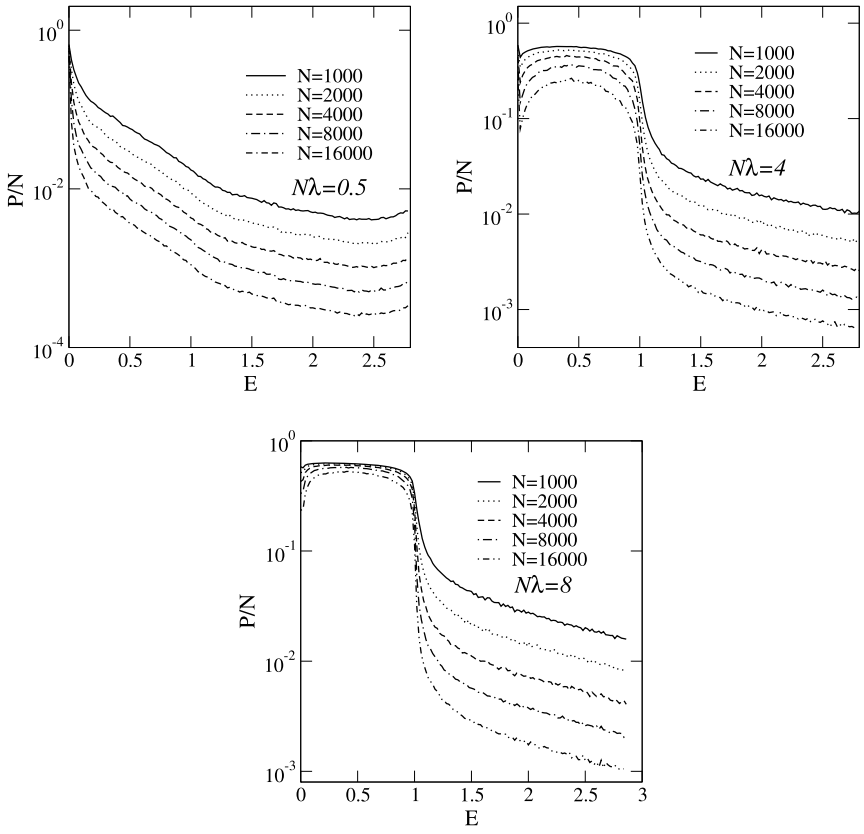

Fig. 5. The mean participation number $P(E)$ versus energy E for $N = 1000$ up to 16000 and $N\lambda = 0.5$, 4 and 8.

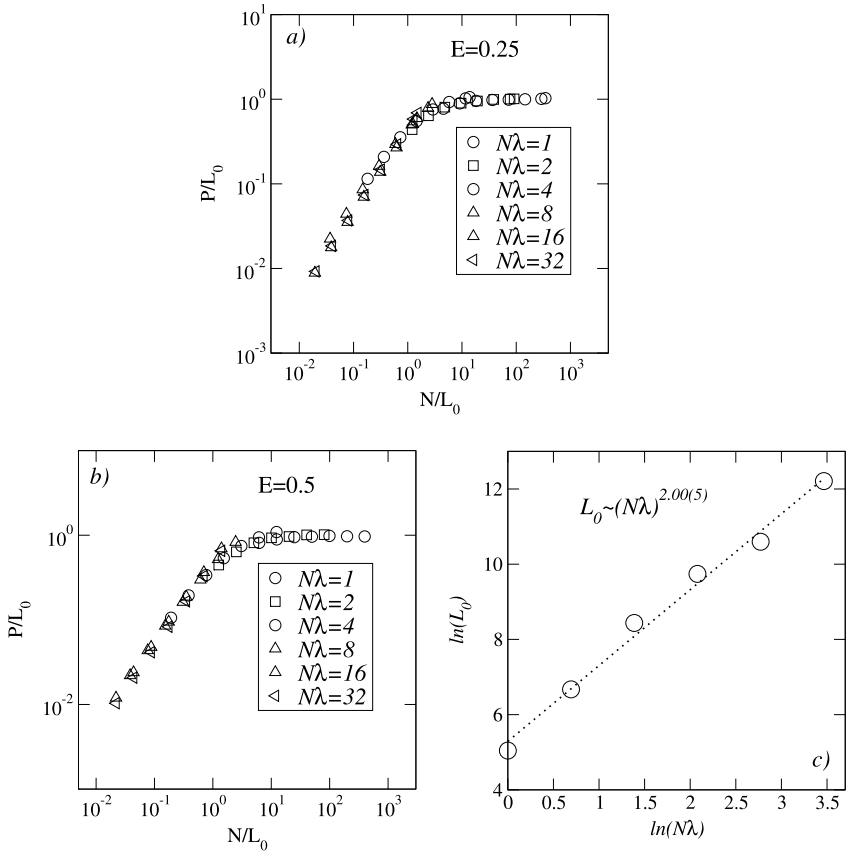

Fig. 6. (a,b) The scaled participation number P/L_0 versus N/L_0 for $E = 0.25$ and $E = 0.5$. The data collapse of all data reveals the finite size scaling of the participation number within the channel. The effective localization length L_0 scales proportional to $(N\lambda)^2$ (see fig. c).

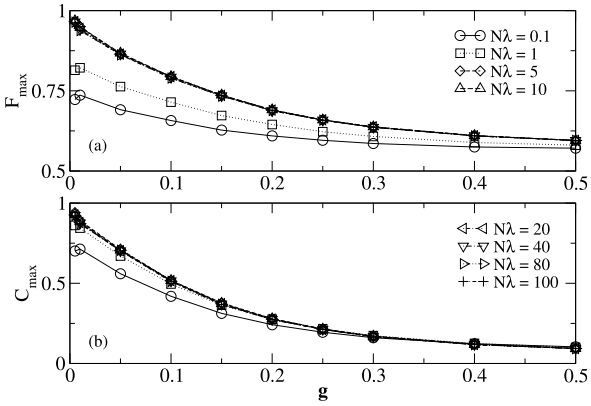

Fig. 7. (a) Maximum fidelity F_{max} as function of g for spin channel with $N = 100$ spins $\epsilon = 0.25$. (b) Maximum concurrence C_{max} as a function of g for the spin channel with $N = 100$ spins $\epsilon = 0.25$.

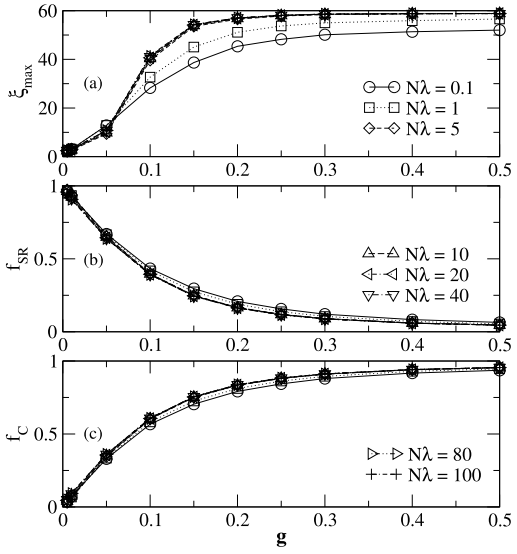

Fig. 8. (a) Maximum participation ξ_{max} as function of g for spin channel with $N = 100$ spins $\epsilon = 0.25$. (b) Mean f_{SR} (Source-Receptor) as function of g for spin channel with $N = 100$ spins $\epsilon = 0.25$. (c) Mean f_C (Channel) as function of g for spin channel with $N = 100$ spins $\epsilon = 0.25$.

encountered for weak coupling. In addition, as shown in Fig. 8.(c), the amplitude of the wave function in the channel region is almost zero, confirming the QST occurrence results at a coupling of $g \approx 0.01$. We stress that this result validates our choice of coupling, which aligns with the values reported in the literature [23]. QST was observed in the initial analysis, even using different values of the correlation length λ for $g \approx 0.01$. The influence of the correlation length $N\lambda$ also becomes relevant when we investigate the behavior of QST as the size of the channel increases.

We will analyze now the dependence on the size of the quantum state transference in our model. We will consider $g = 0.01$ and several values of correlated parameter $N\lambda$. In Fig. 9.(a) we plot a summary of our main results. For an uncorrelated system ($N\lambda < 1$), we observed that the maximum fidelity $F_{\max}$ decreased as N is increased, indicating that QST is absent for larger channels. The same was observed for finding maximum concurrence $C_{\max}$ in Fig. 9.(b), where the entanglement was lost for larger N. In contrast, for correlated systems ($N\lambda > 1$), we observed a high maximum fidelity $F_{\max}$ above 0.9, even for larger channel lengths. Therefore these results suggest that the presence of correlations promotes the existence of quantum state transference with reasonable quality.

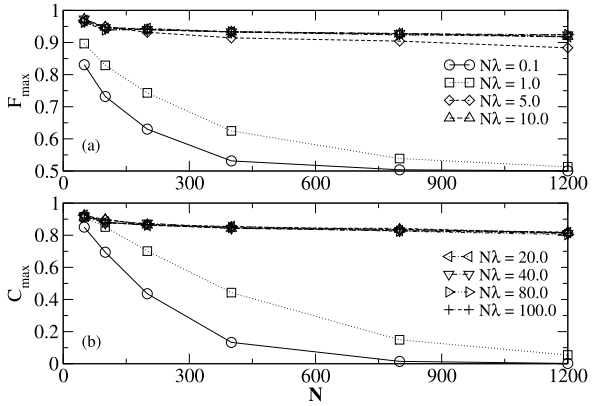

Fig. 9. (a) Maximum fidelity F_{max} as function of N with $\epsilon = 0.25$ and $g = 0.01$. (b) Maximum concurrence C_{max} as function of N with $\epsilon = 0.25$ and $g = 0.01$.

4. Conclusion

In our research, we explored the dynamics of quantum state transfer between two spins connected through a disordered channel. The spin dynamics are governed by a quantum Heisenberg Hamiltonian featuring XYZ symmetry, which allows us to model the intricate behavior of spin interactions in this system. Our study begins by initializing a quantum state localized on the first spin of the model, referred to as the source spin, and then tracking the evolution of this state as it propagates towards the final spin, known as the receiver spin. The disordered channel connecting the source and receiver spins is designed to exhibit intrinsic correlations characterized by exponential decay. This choice of disorder introduces complex variations in the spin coupling strengths throughout the channel, significantly influencing the quantum state transfer process. Our results reveal that in channels with strong correlations, the localization length of states in the low-energy region can become substantially large—comparable to the size of the system itself. This finding suggests that the disorder-induced correlations can significantly impact the quantum state transfer dynamics. To quantify these effects, we performed an extensive finite-size scaling analysis of the localized states within the disordered channel. Our numerical simulations indicate that states with large localization lengths enhance the efficiency of quantum state transfer from the source to the receiver. Specifically, we observed that the quality of quantum state transfer improves with increasing localization length, suggesting a positive correlation between localization and transfer efficiency. Additionally, we investigated how the coupling strength between the channel and the source and receiver spins affects the quality of the quantum state transfer. Our findings demonstrate that the quantum transfer maintains reasonably good fidelity even under weak coupling conditions. This implies that while the coupling strength plays a role in optimizing the transfer process, quantum state transfer can still be effective in scenarios of weak coupling. Overall, our study highlights the critical role of disorder correlations and coupling strength in shaping the efficiency of quantum state transfer in disordered spin chains, offering valuable insights into optimizing quantum communication protocols.

CRediT authorship contribution statement

D.B. Fonseca: Visualization, Validation, Software, Formal analysis, Data curation. **A.L.R. Barbosa:** Investigation, Formal analysis, Conceptualization. **F. Moraes:** Formal analysis, Conceptualization. **G.M.A. Almeida:** Formal analysis, Conceptualization. **F.A.B.F. de Moura:** Writing – original draft, Visualization, Validation, Supervision, Software, Project administration, Methodology, Investigation, Funding acquisition, Formal analysis, Data curation, Conceptualization.

Declaration of competing interest

The authors declare that they have no known competing financial interests or personal relationships that could have appeared to influence the work reported in this paper.

Data availability

Data will be made available on request.

References

[1] Yi-Te Huang, Jhen-Dong Lin, Huan-Yu Ku, Yueh-Nan Chen, Phys. Rev. Res. 3 (Apr 2021) 023038.
[2] Yifei Chen, Licheng Zhang, Yongjian Gu, Zhao-Ming Wang, Phys. Lett. A 382 (39) (2018) 2795–2798.
[3] M. Amazioug, B. Maroufi, M. Daoud, Phys. Lett. A 384 (27) (2020) 126705.
[4] Nahid Binandeh Dehaghani, Fernando Lobo Pereira, IFAC-PapersOnLine 55 (16) (2022) 214–219, 18th IFAC Workshop on Control Applications of Optimization CAO 2022.
[5] Pablo Serra, Alejandro Ferrón, Omar Osenda, Phys. Lett. A 449 (2022) 128362.
[6] Arindam Saha, Amarendra K. Sarma, Phys. Lett. A 393 (2021) 127176.
[7] D.S. Acosta Coden, S.S. Gómez, A. Ferrón, O. Osenda, Phys. Lett. A 387 (2021) 127009.
[8] E.B. Fel'dman, A.N. Pechen, A.I. Zenchuk, Phys. Lett. A 413 (2021) 127605.
[9] Darvin Wanisch, Stephan Fritzsche, Phys. Rev. A 102 (3) (2020) 032624.
[10] Alastair Kay, Int. J. Quantum Inf. 8 (04) (2010) 641–676.
[11] Giulia Gualdi, Vojtech Kostak, Irene Marzoli, Paolo Tombesi, Phys. Rev. A 78 (2) (2008) 022325.
[12] Salvatore Lorenzo, Tony J.G. Apollaro, Andrea Trombettoni, Simone Paganelli, Int. J. Quantum Inf. 15 (05) (2017) 1750037.
[13] Dylan Lewis, Leonardo Banchi, Yi Hong Teoh, Rajibul Islam, Sougato Bose, Ion trap long-range xy model for quantum state transfer and optimal spatial search, Quantum Sci. Technol. 8 (3) (jun 2023) 035025.
[14] M. Akhtar, F. Bonus, F.R. Lebrun-Gallagher, N.I. Johnson, M. Siegele-Brown, S. Hong, S.J. Hile, S.A. Kulmiya, S. Weidt, W.K. Hensinger, High-fidelity quantum matter-link between ion-trap microchip modules, Nat. Commun. 14 (531) (jun 2023) 531.
[15] Catherine Keele, Alastair Kay, Combating the effects of disorder in quantum state transfer, Phys. Rev. A 105 (Mar 2022) 032612.
[16] S. Ashhab, Quantum state transfer in a disordered one-dimensional lattice, Phys. Rev. A 92 (Dec 2015) 062305.
[17] Alexander Duthie, Sthitadhi Roy, David E. Logan, Anomalous multifractality in quantum chains with strongly correlated disorder, Phys. Rev. B 106 (2) (2022) L020201.
[18] D. Messias, C.V.C. Mendes, G.M.A. Almeida, M.L. Lyra, F.A.B.F. de Moura, Rabi-like quantum communication in an aperiodic spin-1/2 chain, J. Magn. Magn. Mater. 505 (2020) 166730.
[19] M.O. Sales, A. Ranciaro Neto, F.A.B.F. de Moura, Spin-wave dynamics in nonlinear chains with spin-lattice interactions, Phys. Rev. E 98 (6) (2018) 062136.
[20] Guilherme M.A. Almeida, Francisco A.B.F. de Moura, Marcelo L. Lyra, Entanglement generation between distant parties via disordered spin chains, Quantum Inf. Process. 18 (2019) 1–15.
[21] D.M. Nunes, A. Ranciaro Neto, F.A.B.F. de Moura, J. Magn. Magn. Mater. 410 (2016) 165.
[22] F.J. Araujo Filho, I.F.F. dos Santos, R.F. Dutra, M.L. Lyra, G.M.A. Almeida, F.A.B.F. de Moura, Quantum Inf. Process. 22 (2023) 327.
[23] Guilherme M.A. Almeida, Francisco A.B.F. de Moura, Marcelo L. Lyra, Quantum-state transfer through long-range correlated disordered channels, Phys. Lett. A 382 (20) (2018) 1335–1340.
[24] Sougato Bose, Quantum communication through an unmodulated spin chain, Phys. Rev. Lett. 91 (20) (2003) 207901.
[25] William K. Wootters, Entanglement of formation of an arbitrary state of two qubits, Phys. Rev. Lett. 80 (10) (1998) 2245.